Advances in Geo-Energy Research

Original article

Aminated nano-silica reinforced slickwater fracturing fluids with enhanced drag reduction, proppant transport and thermal stability

Fei Ding¹⁰*, Caili Dai², Qing You³⁰*, Weichu Yu¹, Yongpeng Sun², Xuguang Song⁴

Keywords:

Nano-reinforcement thermal stability molecular dynamics drag reduction proppant transport slickwater fracturing fluid

Cited as:

Ding, F., Dai, C., You, Q., Yu, W., Sun, W., Song, X. Aminated nano-silica reinforced slickwater fracturing fluids with enhanced drag reduction, proppant transport and thermal stability. Advances in Geo-Energy Research, 2025, 18(2): 153-164.

https://doi.org/10.46690/ager.2025.11.05

Abstract:

Conventional slickwater fracturing fluids undergo severe thermal degradation in hightemperature reservoirs, significantly impairing their drag reduction efficiency and proppant transport capability. To address this limitation, this study presents a novel temperatureresistant slickwater system by incorporating aminated nano-silica with an acrylamide-2acrylamido-2-methylpropane sulfonic acid copolymer and a flowback aid/clay stabilizer. Macroscopic experiments and molecular dynamics simulations reveal that the system achieves a drag reduction rate of 69.7% at 150 °C, a 10-percentage-point improvement over the non-reinforced system. It also reduces the proppant settling area by 21.2%, facilitating more uniform proppant distribution toward the fracture distal end, and retains 77.8% of its initial viscosity after thermal aging. Nanoparticles in the system exhibit a synergistic dualreinforcement mechanism: Their surface adsorption smooths wall roughness and thickens the elastic boundary layer, suppressing turbulence and mitigating energy dissipation; hydrogen bonding and electrostatic interactions between the amino groups of nanoparticles and the moieties of copolymer form an interfacial network, effectively restricting the segmental mobility of the copolymer. This method increases the glass transition temperature of the system by 57.5 °C, markedly enhancing its thermal stability. Molecular simulations confirm an 18.7% increase in hydrogen bond density and a 23.5% reduction in segmental mobility, collectively stabilizing the polymer against thermal degradation. This study provides valuable insights for developing high-performance fracturing fluids suitable for deep reservoirs.

1. Introduction

Shale reservoirs, characterized by low porosity and ultralow permeability, have small natural productivity (Tao et al., 2023). Consequently, large-scale volume fracturing is essential to generate complex fracture networks and establish effective seepage pathways for commercial exploitation (Lei et al., 2023; Wang et al., 2024). Slickwater fracturing fluids, favored for their low drag and ability to induce complex fractures, dominate shale reservoir development (Zhang et al., 2025a). However, as fracturing operations target deeper reservoirs, the thermal vulnerability of conventional slickwater systems becomes increasingly prominent (Li et al., 2021). At elevated temperatures (> 90 °C), core polymer drag reducers undergo main-chain scission and side-group degradation,

Yandy Scientific Press *Corresponding author.

E-mail address: dingfei@yangtzeu.edu.cn (F. Ding); daicl@upc.edu.cn (C. Dai); youqing@cugb.edu.cn (Q. You); yuweichu@126.com (W. Yu); sunyongpeng@upc.edu.cn (Y. Sun); xuguang1@ualberta.ca (X. Song). 2207-9963 © The Author(s) 2025.

Received August 16, 2025; revised September 12, 2025; accepted October 7, 2025; available online October 11, 2025.

¹College of Chemistry & Environmental Engineering, Yangtze University, Jingzhou, 434023, P. R. China

²School of Petroleum Engineering, China University of Petroleum (East China), Qingdao 266580, P. R. China

³School of Energy Resources, China University of Geosciences (Beijing), Beijing 100083, P. R. China

⁴Department of Chemical and Materials Engineering, University of Alberta, Edmonton AB T6G 1H9, Canada

significantly impairing drag reduction efficiency and viscosity (Xiong et al., 2018; Zhao et al., 2024; Zuo et al., 2025). This degradation not only limits the effective treatment radius but also increases the risk of premature proppant settling and fracture channel blockage, severely compromising stimulation outcomes (Yang et al., 2019; Zhang et al., 2019). Thus, heat-resistant slickwater fracturing fluids are in critical demand for deep reservoir exploitation.

Nano-silica offers a promising solution to these challenges. By forming nanocomposite systems with polymer drag reducers, it remarkably enhances the high-temperature drag reduction and proppant transport performance of slickwater fracturing fluids (Giraldo et al., 2017; Hu et al., 2019; Liu et al., 2020; Zhang et al., 2025b). Previously proposed thermostabilizing mechanisms include (Cao et al., 2018; Haruna et al., 2020; Liu et al., 2021; Yuan et al., 2023): (1) The high specific surface area of nano-silica facilitates polymer chain adsorption onto its surface, forming a "boundary layer" that restricts the thermal motion of polymer segments; (2) surfacefunctionalized groups interact with polymer molecules via hydrogen bonding, electrostatic forces, and covalent linkages, ensuring the uniform dispersion of nano-silica within the polymer network to reinforce structural integrity and dissipate thermal energy; and (3) surface hydroxyl groups scavenge thermally generated free radicals (e.g., hydroxyl and methylene radicals), thereby retarding degradation chain reactions. Despite these advances, the dynamic enhancement mechanisms of nanoparticles in turbulent flow fields and their molecularlevel interactions with polymers remain rarely studied.

To bridge the above research gap, this study introduces a supramolecular-engineered nanocomposite system integrating aminated nano-silica with copolymer of acrylamide and 2acrylamido-2-methylpropane sulfonic acid, and systematically investigates its performance via experimental and molecular theoretical approaches. Specifically, a novel nanocomposite slickwater fracturing fluid (Slickwater-NPAS) is proposed. By leveraging supramolecular interactions, this system achieves enhanced drag reduction and proppant transport performance under high-temperature conditions. The enhancement mechanisms of nanoparticles on the performance of slickwater fracturing fluid are elucidated through a combination of macroscale testing (drag reduction efficiency, dynamic proppant transport capacity, and viscosity measurements), microstructural characterization (scanning electron microscopy and particle image velocimetry), and molecular dynamics simulations. The findings of this study provide critical insights for developing high-performance fracturing fluids tailored for deep reservoir applications.

2. Materials and methods

2.1 Materials

NPAS was formulated by incorporating 20.0 wt% aminografted nano-silica into PAS (Ding et al., 2023), a copolymer of acrylamide and 2-acrylamido-2-methylpropane sulfonic acid. JHFR-1 and JHFR-2 are two water-in-water emulsion drag reducers (Jingzhou Modern Petroleum Technology Development Co., Ltd., Jingzhou, China). JHFR-2D is a multifunc-

tional additive acting as both a flowback aid and clay stabilizer (Jingzhou Modern Petroleum Technology Development Co., Ltd., Jingzhou, China). Quartz sand with particle sizes of 40-70 mesh (density: 1.45 g/cm³) and 70-140 mesh (density: 2.02 g/cm³) was used as the proppant (Lingshou Huachen Mineral Products Trading Co., Ltd., Shijiazhuang, China). NaCl, KCl, MgCl₂, and CaCl₂ were commercially purchased (Shanghai Macklin Biochemical Technology Co., Ltd., Shanghai, China). The standard brine (total salinity 82,612.0 mg/L) consisted of 2.0 wt% KCl, 5.5 wt% NaCl, 0.45 wt% MgCl₂, and 0.55 wt% CaCl₂. The simulated formation water (total salinity 57,249.0 mg/L) had the following ionic composition: 20,800 mg/L (Na⁺+K⁺), 1,202 mg/L Ca²⁺, 159 mg/L Mg²⁺, 34,421 mg/L Cl⁻, and 62 mg/L SO₄²⁻.

2.2 Preparation of slickwater fracturing fluids

The slickwater fracturing fluids developed in this study (Slickwater-PAS and Slickwater-NPAS) consisted of a drag reducer (PAS or NPAS, respectively; typically, at a concentration of 0.10 wt%) and the additive JHFR-2D. For drag reduction and rheological performance tests, the drag reducer concentration was adjusted according to the experimental requirements, while the dosage of JHFR-2D was kept constant at 0.2 vol% across all formulations.

2.3 Characterizations

2.3.1 Microscopic morphology of aminated nano-silica particles

The morphology of aminated nano-silica particles was characterized using transmission electron microscopy (TEM) (JEM2100plus, JEOL Ltd., Tokyo, Japan). Briefly, an ethanol dispersion of the nanoparticles was prepared and ultrasonically treated for 30 min to ensure uniform dispersion. An aliquot of the dispersion was pipetted onto a copper grid, air-dried under ambient conditions to prepare the TEM sample, and then imaged via TEM.

2.3.2 Hydrodynamic radius of aminated nano-silica particles

The hydrodynamic radius of the nanoparticles was measured via dynamic light scattering (DLS) (Omni-1, Brookhaven Instruments Corporation, New York, America). For sample preparation, the aqueous nanoparticle solution was ultrasonically agitated and filtered through a 0.22 μm microporous membrane to remove agglomerates. A suitable volume of the filtered solution was transferred into a clean DLS sample cell using a micropipette, followed by DLS measurement.

2.3.3 Microscopic morphology of Slickwater-NPAS

The microscopic morphology of Slickwater-NPAS was observed via atomic force microscopy (AFM) (Multimode 8, Bruker Co., Ltd., Saarbrucken, Germany). Slickwater-NPAS was prepared at the designed concentration, and an appropriate amount was deposited onto a mica sheet to form a thin film. The sample was freeze-dried for 24 h (SCIENTZ-10N, Ningbo Xinchi Biological Technology Co., Ltd., Ningbo, China). AFM

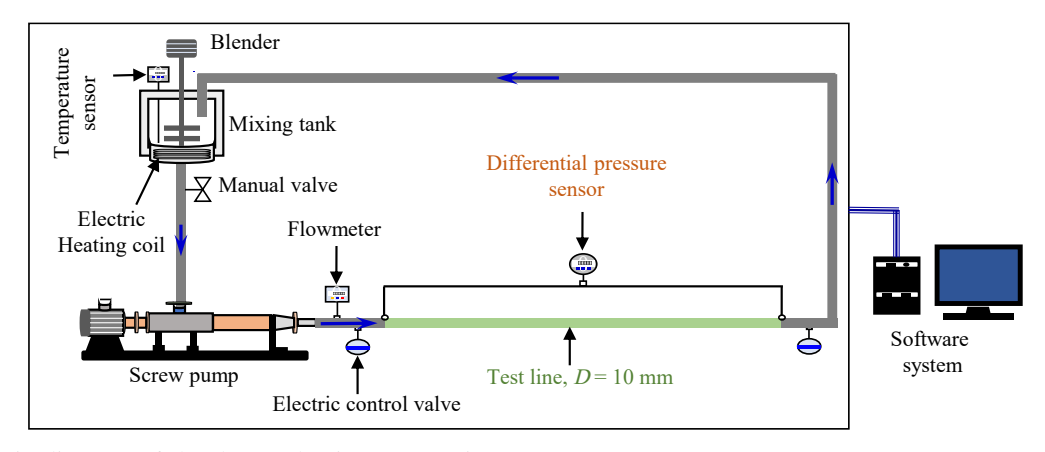


Fig. 1. Schematic diagram of the drag reduction rate testing process.

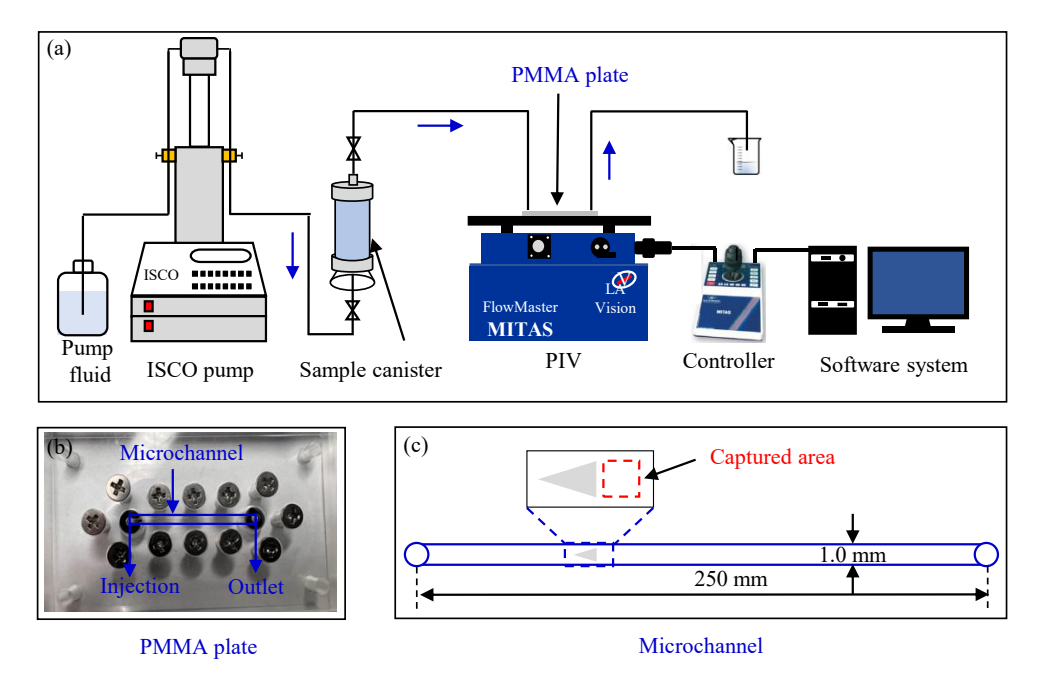


Fig. 2. Schematic diagram of (a) microflow field distribution testing, (b) physical image of PMMA plate and (c) schematic diagram of microchannel.

imaging was performed in tapping under ambient conditions (25 °C, 30% relative humidity).

2.3.4 Drag reduction performance

Drag reduction performance was evaluated using a high-temperature/high-pressure drag resistance tester (CQJZ-DM, Jiangsu Huaan Scientific Instruments Co., Ltd., Nantong, China). This system measures the pressure drop (ΔP) along a 4.5 m test section. The drag reduction rate (DR, %) was calculated using the following equation (Jouenne et al., 2015; Ibrahim et al., 2018):

$$DR = \frac{\Delta P_0 - \Delta P_1}{\Delta P_0} \times 100 \tag{1}$$

where ΔP_0 and ΔP_1 denote the pressure drops for fresh water and the drag reducer solution, respectively, and a higher DR indicates superior drag reduction efficiency. A schematic of the testing setup is shown in Fig. 1.

Particle Image Velocimetry (LaVision, Göttingen, Germany) was performed to visualize flow patterns in a microchannel with triangular obstacles (Fig. 2(a)) (Xu et al., 2023). The microchannel was fabricated on a polymethyl methacrylate (PMMA) plate (Fig. 2(b)). A triangular obstacle (leg length: 2.52 mm; base length: 0.6 mm) was designed to induce turbulence (Fig. 2(c)), where the imaging area (400 μ m \times 400 μ m) is marked by a red box.

2.3.5 Rheological viscosity

The viscosity of the slickwater fracturing fluids was measured using a high-temperature/high-pressure rheometer (HAAKE MARS 60, Thermo Fisher Scientific, Waltham, USA).

2.3.6 Proppant transport performance

A visual plate fracture model (1.2 m \times 50 cm \times 6 mm) was used to characterize the dynamic proppant dis-

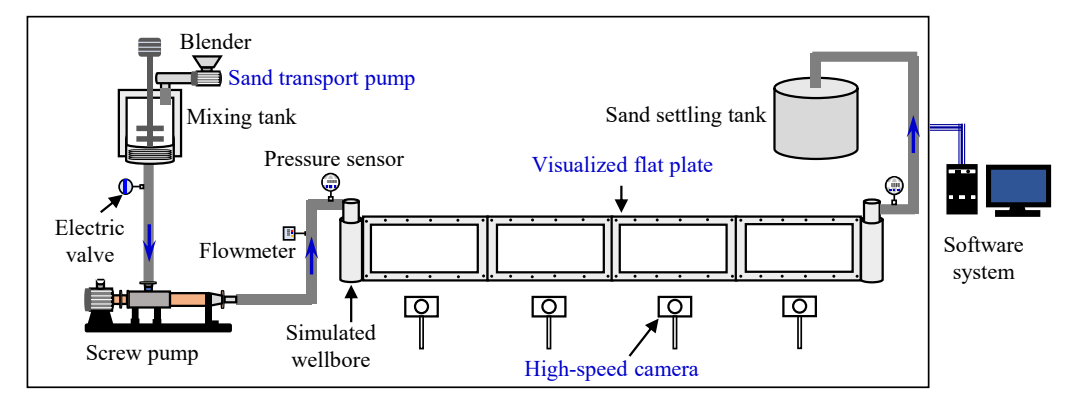


Fig. 3. Flow schematic of dynamic proppant transport experimental equipment.

tribution under flow conditions (CQJZ-DM, Jiangsu Huaan Scientific Instruments Co., Ltd., Nantong, China) (Alotaibi and Miskimins, 2018; Isah et al., 2021). The proppant settling area and bank height were quantified via image processing techniques. All test fluids were thermally aged at 150 °C for 2 h prior to testing. A photograph of the physical apparatus and a flow schematic are presented in Fig. 3, respectively. The proppant concentrations (5 vol% and 15 vol%) and particle sizes (40-70 mesh and 70-140 mesh) employed in this study were referenced to the sand concentrations and proppant particle sizes of field-scale. Additionally, the flow rates used in the experiments were determined by simulating the linear velocity of fracturing fluids under field conditions, performed in accordance with similarity criteria.

2.3.7 Temperature resistance properties

The *DR* of Slickwater-PAS and Slickwater-NPAS under different temperature conditions were determined using a high-temperature/high-pressure drag resistance tester.

The viscosity of the slickwater fracturing fluids at various temperatures was measured using a high-temperature/high-pressure rheometer. The viscosity retention rate (η_R) was calculated using:

$$\eta_R = \frac{\eta_T}{\eta_0} \times 100\% \tag{2}$$

where η_0 and η_T denote the viscosities measured at 30 °C and elevated temperatures, respectively.

Field emission scanning electron microscopy (Quanta FEG250, FEI, USA) was used to observe the microstructure of the samples. The slickwater fracturing fluids were thermally aged in an oven at 150 °C for 2 h. After cooling, the samples were freeze-dried for 48 h. Prior to imaging, they were sputter-coated with gold to enhance conductivity.

2.4 Molecular dynamics simulations

Molecular dynamics simulations were performed using Materials Studio software with the COMPASS force field. Newton's equations of motion were integrated via the Velocity Verlet algorithm. All simulations were conducted under the NPT ensemble (constant number of particles, pressure, and temperature), where temperature and pressure were controlled by the Nosé-Hoover thermostat and Berendsen method, re-

spectively. Van der Waals interactions were calculated using an atom-based method with a cutoff radius of 12.5 Å, while long-range electrostatic interactions were handled via the Ewald summation method. The simulation time step was set to 1 fs, and trajectories were recorded every 1 ps. Periodic boundary conditions were applied along all directions (x, y, and z axes).

The initial PAS and NPAS models were subjected to NPT ensemble simulations as follows: first, simulations were run at 108 K and 1 MPa for 1,000 ps, followed by heating to 900 K for 3,000 ps. Subsequently, the systems were cooled stepwise to 300 K at a rate of 25 K per 1,000 ps. For each temperature step, the last 100 ps of the trajectory was analyzed to determine the volume and dynamic properties of the systems. This entire simulation procedure was repeated three times using reconstructed models, and the results were averaged to ensure statistical reliability. Mean square displacement (MSD) analysis is a key method for characterizing polymer segmental mobility. The MSD of the polymer chains in PAS and NPAS was calculated over a 200 ps duration at 600 K.

3. Results and discussion

3.1 Preparation of Slickwater-NPAS

Slickwater fracturing fluid is primarily composed of water (>99.0 wt%) and minor chemical additives (<1.0 wt%) (Fig. 4(a)), with the drag reducer serving as its core component. During fracturing operations, large volumes of fluid invade the formation matrix through the fracture network under capillary forces and become trapped. This can induce formation damage via mechanisms such as fluid retention and clay swelling, impairing well productivity. Consequently, flowback is required to remove the fluid. Incorporating a flowback aid effectively reduces the fluid's surface and interfacial tension, facilitating flowback. Additionally, the hydration and swelling of rock minerals upon contact with water may cause pore-throat constriction and particle detachment/migration, further exacerbating formation damage.

This study employs slickwater fluid systems (Slickwater-PAS or Slickwater-NPAS) consisting of a drag reducer (either PAS or NPAS) and a multifunctional additive, JHFR-2D, which acts as both a flowback aid and clay stabilizer (Fig. 4(a)). PAS is an emulsion copolymer of acrylamide and

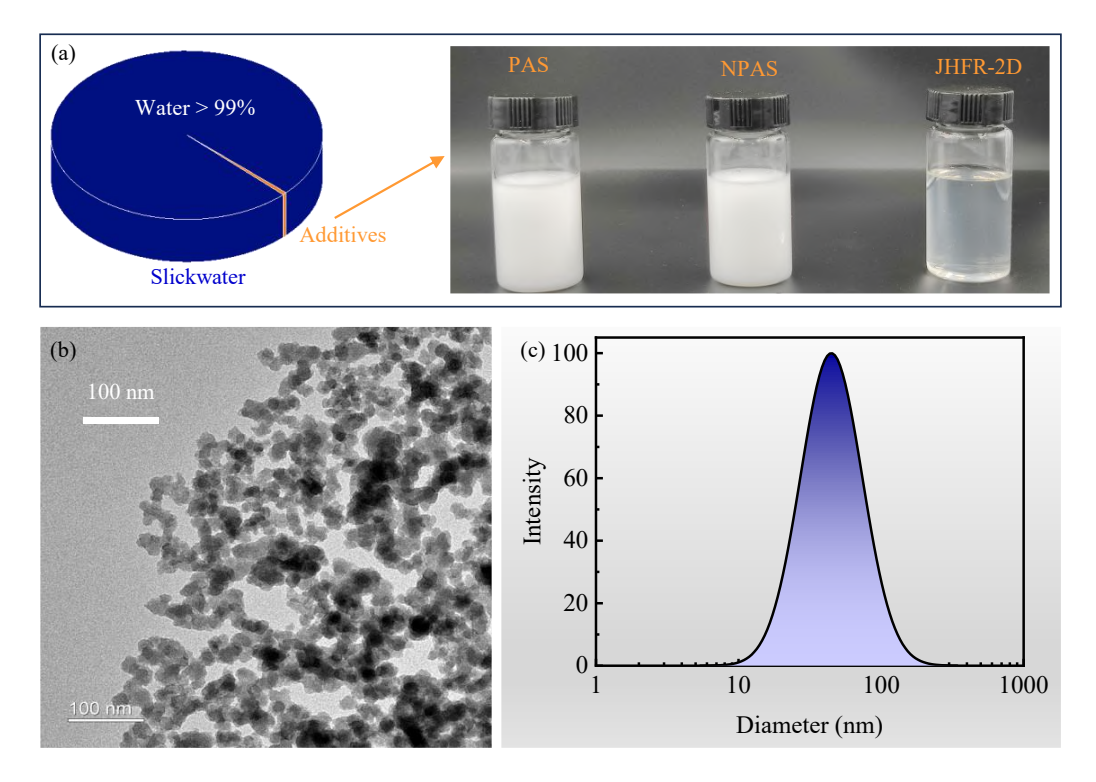


Fig. 4. Appearance of (a) PAS, NPAS and JHFR-2D, (b) TEM image and (c) hydrodynamic radius distribution of aminated nano-silica particles.

2-acrylamido-2-methylpropane sulfonic acid synthesized via aqueous two-phase polymerization. NPAS differs from PAS by incorporating aminated modified nano-silica (Fig. 5(a)), the nano-silica has a particle size of 10-20 nm (Fig. 4(b)) and a hydrodynamic radius D_{50} of 41.99 nm (Fig. 4(c)).

The microscopic morphology of Slickwater-NPAS was observed via AFM. In the image, brightness corresponds to the adsorption height of the sample on the mica sheet surface, with higher indicating greater height. Low-magnification AFM images (Figs. 5(b) and 5(d)) reveal numerous high-contrast features. Corresponding high-magnification images (Figs. 5(c) and 5(e), showing the blue boxed regions in Figs. 5(b) and 5(d), respectively) demonstrate that the strip-like structures are nanoparticle aggregates uniformly dispersed in Slickwater-NPAS. This confirms the successful synthesis of NPAS, consistent with our previous study (Ding et al., 2023).

3.2 Drag reduction performance

During injection, significant turbulence in fracturing fluid dissipates kinetic energy, thereby reducing the energy available for effective reservoir fracturing. Polymer drag reducers mitigate turbulence, substantially decreasing drag in extended wellbores.

Drag reduction arises from interactions between polymers and turbulent eddies, with its efficiency highly dependent on molecular concentration and aggregation state (Dunlop and Cox, 1977; Shetty and Solomon, 2009). For both Slickwater-PAS and Slickwater-NPAS, *DR* increased significantly with concentration up to 0.10 vol%, rising from 61.3% and 63.5% at 0.025 vol% to 74.4% and 76.1% at 0.10 vol%, respectively

(Figs. 6(a) and 6(b)). Beyond this concentration, DR plateaued, which can be attributed to three factors: (1) an insufficiency of drag reducer molecules to suppress eddies effectively at low concentrations; (2) enhanced eddy suppression and increased DR with rising concentration; (3) molecular entanglement at excessive concentrations, which restricts chain extension and limits further DR improvements.

Cations in the formation fluids (e.g., Na⁺, Ca²⁺) or adsorbed on the rock surface can interact electrostatically with functional groups of fracturing fluid additives. This interaction may alter molecular conformation or induce charge shielding, potentially impairing performance. Fig. 6(c) compares the DR values in tap water, simulated formation water, and standard brine. It can be seen that DR decreases with increasing salinity: initial values were 75.5%, 74.7%, and 73.9%, dropping to 74.3%, 72.7%, and 72.2% after 5 min of shearing, and further to 70.5%, 69.2%, and 68.5% after 10 min. Notably, the effective drag reduction performance is maintained even in high-salinity brine. This can be ascribed to the strong electrostatic repulsion from sulfonic acid groups in molecular chains of NPAS, coupled with steric hindrance from the bulky side chains of AMPS. These two factors collectively suppress molecular chains curling.

The enhancing effect of nanoparticles on drag reduction efficiency was further investigated using Particle Image Velocimetry to characterize flow distribution. Flow patterns were visualized in a microchannel with turbulence-inducing triangular obstacles. In fresh water, flow separation with pronounced recirculation zones was observed near the walls, yielding an average velocity of 0.17 m/s (Figs. 6(d), 6(e), and 6(f)).

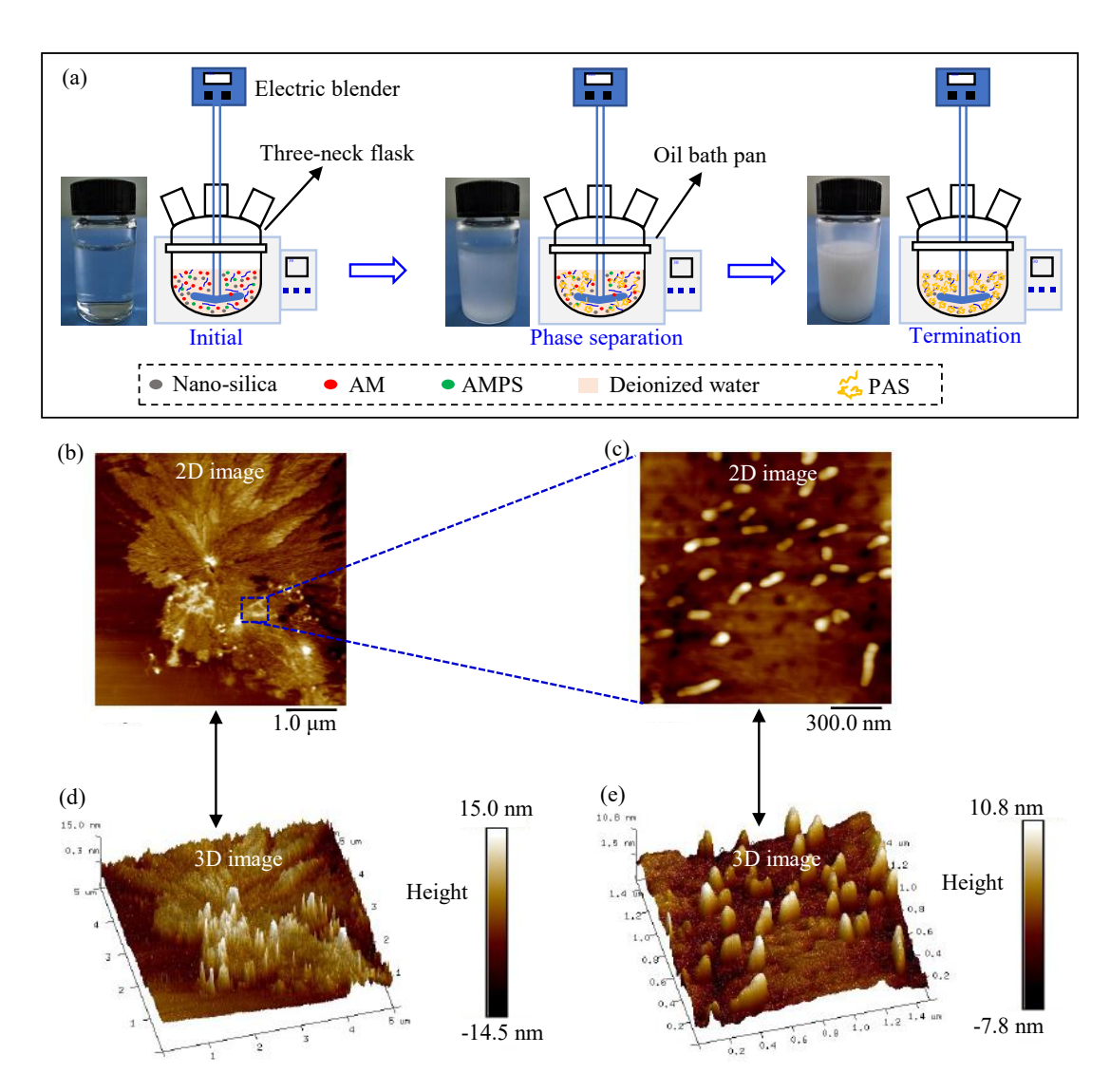


Fig. 5. Schematic diagram of (a) the NPAS synthesis process and (b)-(e) the microscopic morphology of Slickwater-NPAS.

Slickwater-PAS exhibited an extended flow field coverage with wall-convergent structures, achieving a higher average velocity of 0.37 m/s (Figs. 6(g), 6(h), and 6(i)). Slickwater-NPAS demonstrated the most homogeneous velocity distribution (Figs. 6(j), 6(k), and 6(l)), reaching the highest average velocity of 0.48 m/s. These PIV results quantitatively confirm the superior turbulence suppression capability of nanoparticles, which directly correlates with the enhanced macroscopic drag reduction observed (Asidin et al., 2019; Xi, 2019; Ou et al., 2024).

3.3 Rheological viscosity

Low-viscosity fracturing fluids facilitate the formation of highly complex fracture networks. This is because higher viscosity increases flow resistance within fractures, hindering deep penetration and reducing effective coverage. Consequently, optimizing slickwater viscosity is a critical task.

Figs. 7(a), 7(b) and 7(c) depict the viscosity-time profiles of slickwater fracturing fluids formulated with PAS and NPAS at different concentrations, measured at a shear rate of 170

s⁻¹ and 25 °C. Viscosity increased with drag reducer concentration but remained low (≤ 26.0 mPa·s at 2.0 vol%). This increase stems from enhanced polymer chain entanglement density and network formation (Kulicke et al., 1982; Ghannam and Esmail, 1998). Notably, Slickwater-NPAS consistently exhibited higher viscosity than Slickwater-PAS at the same concentration, with the viscosity difference increasing as concentration rose (from 0.3 mPa·s at 0.1 vol% to 2.5 mPa·s at 2.0 vol%). This enhancement is attributed to increased nanoparticle loading, which strengthens hydrogen bonding and electrostatic interactions, thereby expanding the hydrodynamic volume of the polymer network (Yegane et al., 2020; Xu et al., 2022).

Figs. 7(d), 7(e) and 7(f) present the viscosity-shear rate curves of Slickwater-PAS and Slickwater-NPAS at 25 °C. Both systems displayed typical shear-thinning behavior: Viscosity decreased initially and then plateaued as the shear rate increased. At low shear rates, however, polymer chains aligned and potential scission occurred, disrupting the network and reducing viscosity.

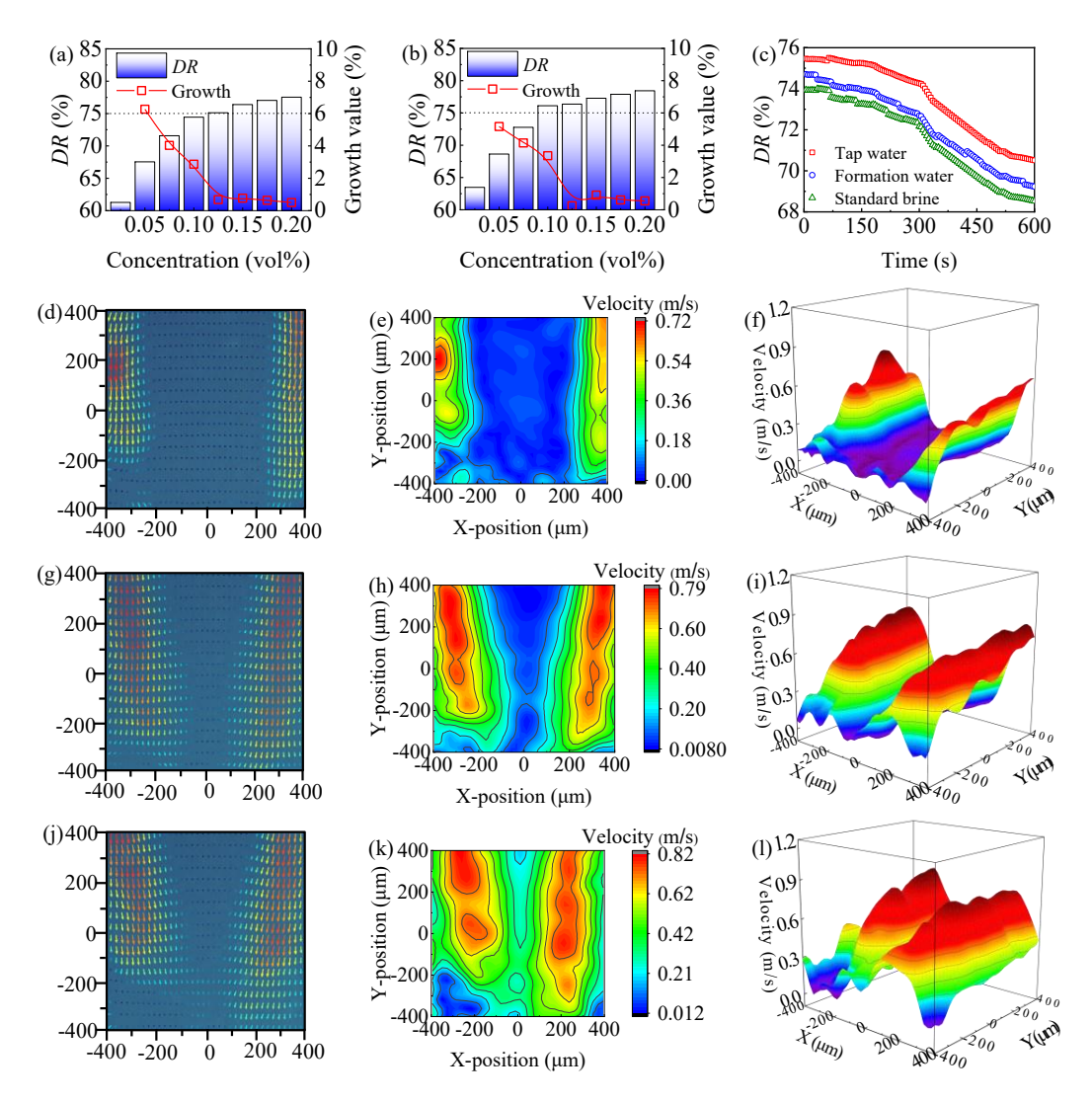


Fig. 6. *DR* curves of (a) Slickwater-PAS and (b) Slickwater-NPAS under different concentrations, *DR* curves (c) under brine conditions, (d) micro flow field of fresh water, (g) Slickwater-PAS and (j) Slickwater-NPAS, and (e)-(f) 2D/3D velocity fields of fresh water, (h)-(i) Slickwater-PAS and (k)-(l) Slickwater-NPAS.

3.4 Proppant transport performance

Effective proppant transport is critical to stimulation success. Low-viscosity slickwater relies on high flow rates and large volumes to suspend proppants, making conventional static evaluation methods inadequate. This study conducted dynamic proppant transport experiments using a visual fracture model.

Figs. 8(a) and 8(b) show the proppant bank morphology and height profile of Slickwater-NPAS at proppant concentrations of 5 vol% and 15 vol%, respectively. The integration of height curve for the 15 vol% case (Fig. 8(f)) yielded a proppant bank volume of 18.7 cm³, occupying 58.3% of the fracture model volume—representing a 36.2-percentage-point increase in model occupancy compared to the 5 vol% case. These results indicate that while Slickwater-NPAS is effective at lower proppant concentrations, it has limited capacity to transport high proppant concentrations without significant premature settling. Figs. 8(c) and 8(g) illustrate the settling behavior of coarser 40-70 mesh proppant in Slickwater-NPAS.

The proppant bank volume occupied 26.1% of the model, a 4.0-percentage-point increase compared to finer 70-140 mesh sand, demonstrating reasonably effective transport for both proppant size ranges under the tested conditions. Figs. 8(d) and 8(h) show the performance of Slickwater-NPAS at a reduced flow rate (50 L/min). The proppant bank volume occupied 38.8% of the model, a 16.7-percentage-point increase relative to the 100 L/min case, clearly demonstrating that increasing the flow rate enhances the proppant transport capability of slickwater.

Figs. 8(a) and 8(e) compare the proppant distribution performance of Slickwater-PAS and Slickwater-NPAS (via proppant bank morphology), quantified using height distribution profiles. Integrating these profiles (Fig. 8(i)) revealed similar total proppant bank volumes for both systems (22% model occupancy). However, a critical difference was observed in spatial distribution: within the near-wellbore fracture section (0-2,400 mm), the settled proppant volume accounted for 67.5% of the total bank volume for Slickwater-PAS, compared to only

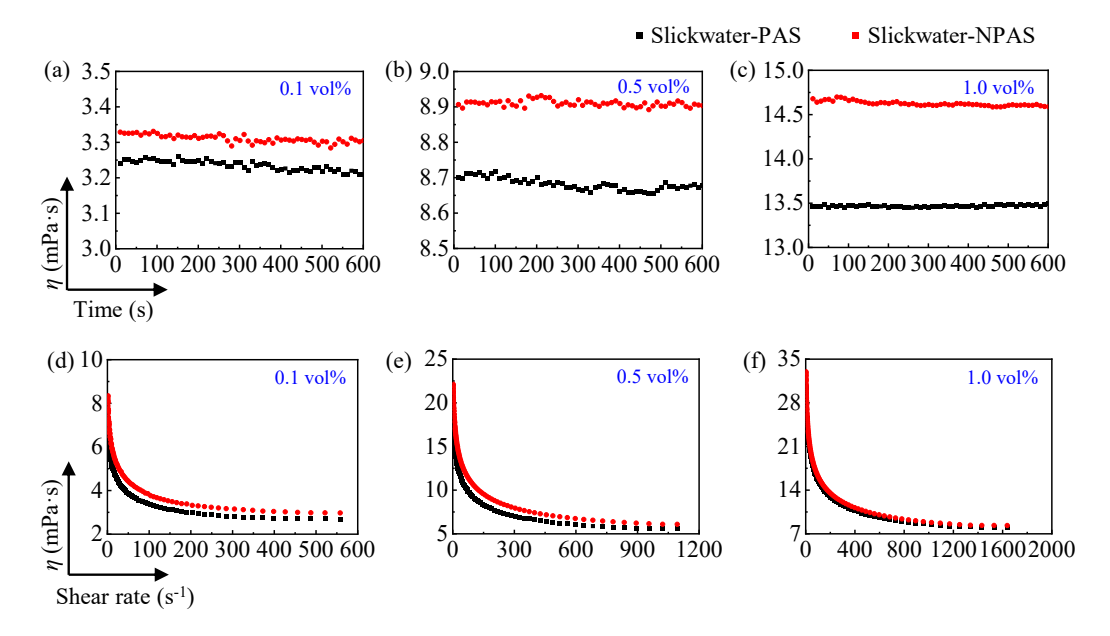


Fig. 7. Viscosity of slickwater fracturing fluids at different (a)-(c) concentrations and (d)-(f) shear rates.

46.3% for Slickwater-NPAS. This indicates that Slickwater-PAS tends to cause proppant settling in the proximal (near-wellbore) region, whereas Slickwater-NPAS transports proppants more toward the fracture distal end—confirming its superior proppant transport capacity. This enhancement is driven by two synergistic mechanisms (Fig. 8(j)): (1) Nanoparticles preferentially adsorb onto micro-asperities on the fracture wall, reducing effective surface roughness and inducing wall slipperiness (Brostow, 2008; Asidin et al., 2019); and (2) PAS forms a viscoelastic boundary layer that dampens turbulent kinetic energy dissipation. Within this layer, nanoparticles act as physical crosslinkers, reinforcing the layer through multiple hydrogen bonds with polymer chains. This thickens the effective shear-thinning film and enhances energy retention for proppant suspension (Brostow, 2008; Asidin et al., 2019).

3.5 Temperature resistance properties

Maintaining high DR at elevated temperatures is crucial for forming complex fracture networks and ensuring adequate fluid coverage. Fig. 9(a) presents the DR of slickwater fracturing fluids formulated with Slickwater-PAS, Slickwater-NPAS, and two water-in-water emulsion drag reducers (i.e., JHFR-1 and JHFR-2) under varying temperature conditions, with the drag reducer concentration fixed at 0.10 vol\%. As temperature increased, a consistent decrease in DR was observed across all tested systems. For illustration, the DR values of JHFR-1, JHFR-2, Slickwater-PAS, and Slickwater-NPAS declined from 72.3%, 75.2%, 74.4%, and 76.1% at 30 °C to 70.3%, 67.3%, 72.5%, and 74.3% at 90 °C, and further decreased to 65.7%, 62.1%, 63.3%, and 69.7% at 150 °C, respectively. This decline arises from the dependence of polymer drag reduction efficacy on molecular chain extension and molecular weight (Zhang et al., 2019): Elevated temperatures induce chain scission and weaken hydrogen bonding between polymer chains and water molecules (Kamel and Shah, 2009), thereby causing chain contraction and reducing drag reduction capability. Importantly, the incorporation of nanoparticles significantly enhanced the thermal stability of the slickwater system, as evidenced by the consistently higher *DR* of Slickwater-NPAS throughout the entire temperature range.

Thermal stability evaluations at a drag reducer concentration of 1.0 vol% revealed significant differences between the two systems (Figs. 9(b) and 9(c)). The viscosity of Slickwater-PAS decreased from 14.6 mPa·s at 30 °C to 9.5 mPa·s at 150 °C, corresponding to a viscosity retention rate of 65.1%. In contrast, Slickwater-NPAS maintained a viscosity of 12.4 mPa·s at 150 °C, with a retention rate of 77.8%. Microscopic observations of slickwater samples aged at 150 °C revealed distinct aggregation morphologies. Slickwater-PAS (Figs. 9(d), 9(e), 9(f) and 9(g)) exhibited disrupted polymer networks with few intact structures remaining; the morphology was characterized by loose, porous architectures and irregular aggregates, resulting from chain agglomeration upon thermal degradation. Conversely, Slickwater-NPAS (Figs. 9(h), 9(i), 9(j) and 9(k)) predominantly displayed intact and compact network frameworks, with markedly fewer fractured domains. This morphological evidence confirms that aminated nano-silica reinforces the polymeric network structure of PAS, thereby enhancing thermal stability and preserving both absolute viscosity and the viscosity retention ratio (Lewandowska, 2007; Yang et al., 2013; ?, ?). This structural integrity underlies the sustained drag reduction and proppant transport capabilities of Slickwater-NPAS under high-temperature conditions.

3.6 Insights into the high-temperature resistance mechanism

To elucidate the origin of the observed macroscopic enhancements in thermal properties – specifically drag reduction and proppant transport capacity – molecular dynamics simulations were employed to probe nanoparticle-

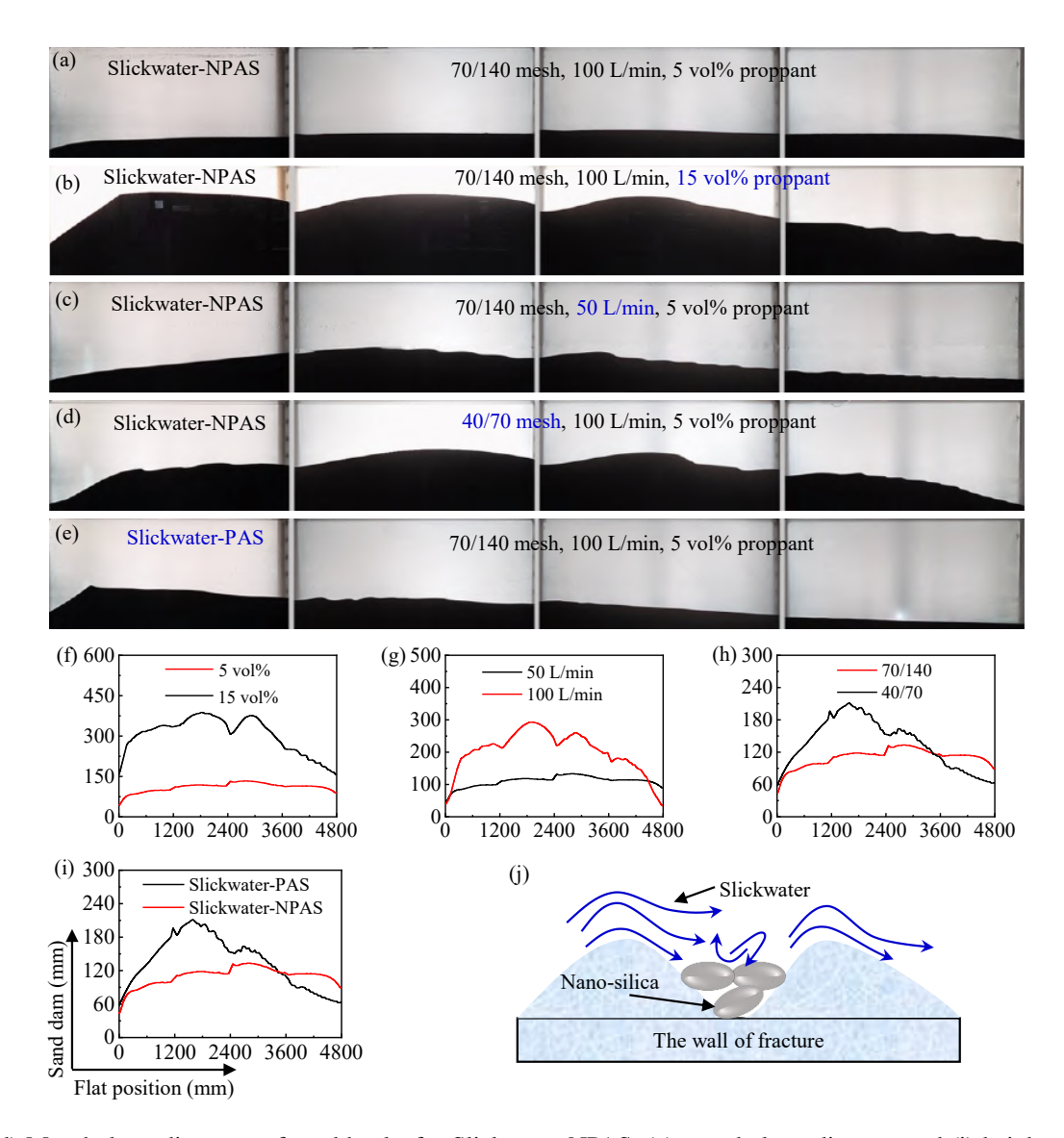


Fig. 8. (a)-(d) Morphology diagrams of sand banks for Slickwater-NPAS, (e) morphology diagram and (i) height curve of sand bank for Slickwater-PAS, (f) height curves of sand bank for Slickwater-NPAS under different sand ratios, (g) flow rates, and (h) proppant meshes, and (j) schematic diagram of nano-silica filling depressions on the fracture wall surface.

polymer interactions and network stabilization mechanisms at the molecular level. Spherical nano-silica aggregates (radius 10 Å) were modeled by truncating bulk α -quartz. Surface oxygen atoms were grafted onto silicon free radicals to simulate oxidation. Subsequently, 20 out of 100 surface oxygen radicals were randomly selected for covalent bonding with γ -aminopropyltriethoxysilane (to simulate aminofunctionalization), while the remaining oxygen radicals were saturated with hydrogen atoms (Fig. 10(a)). The PAS matrix was modeled using AM6AMPS4 chains (Fig. 10(b)). The NPAS composite structure was constructed by embedding a single nanoparticle at the center, surrounded by 40 AM6AMPS4 chains (Fig. 10(c)). The control PAS model contained only 40 AM6AMPS4 chains (Fig. 10(d)). To ensure charge neutrality, Na⁺ counterions were added to both systems.

The calculated glass transition temperature (T_g) for PAS was 536.37 K, compared to 593.86 K for NPAS (Fig. 10(e)),

representing a substantial increase of 57.5 °C. NPAS also exhibited higher density than PAS across the temperature range, indicating that nano-silica incorporation densifies the PAS network, thereby enhancing thermal stability. To assess the effect of nano-silica on molecular mobility, the MSD of PAS and NPAS chains was calculated (Fig. 10(f)). NPAS exhibited significantly reduced atomic mobility, with MSD values 23.5% lower than those of PAS at 600 K. The steeper slope of the PAS MSD curve further confirms restricted segmental motion in NPAS, demonstrating that nanoparticles effectively suppress thermal fluctuations within the polymer matrix. Using equilibrated models at 300 K, hydrogen bond analysis was performed over a 100 ps trajectory. NPAS formed 18.7% more intermolecular hydrogen bonds than PAS (Fig. 10(g)). Complementary electrostatic charges between the protonated amino groups on nano-silica and the dissociated sulfonic acid groups on PAS drive strong electrostatic interactions. The

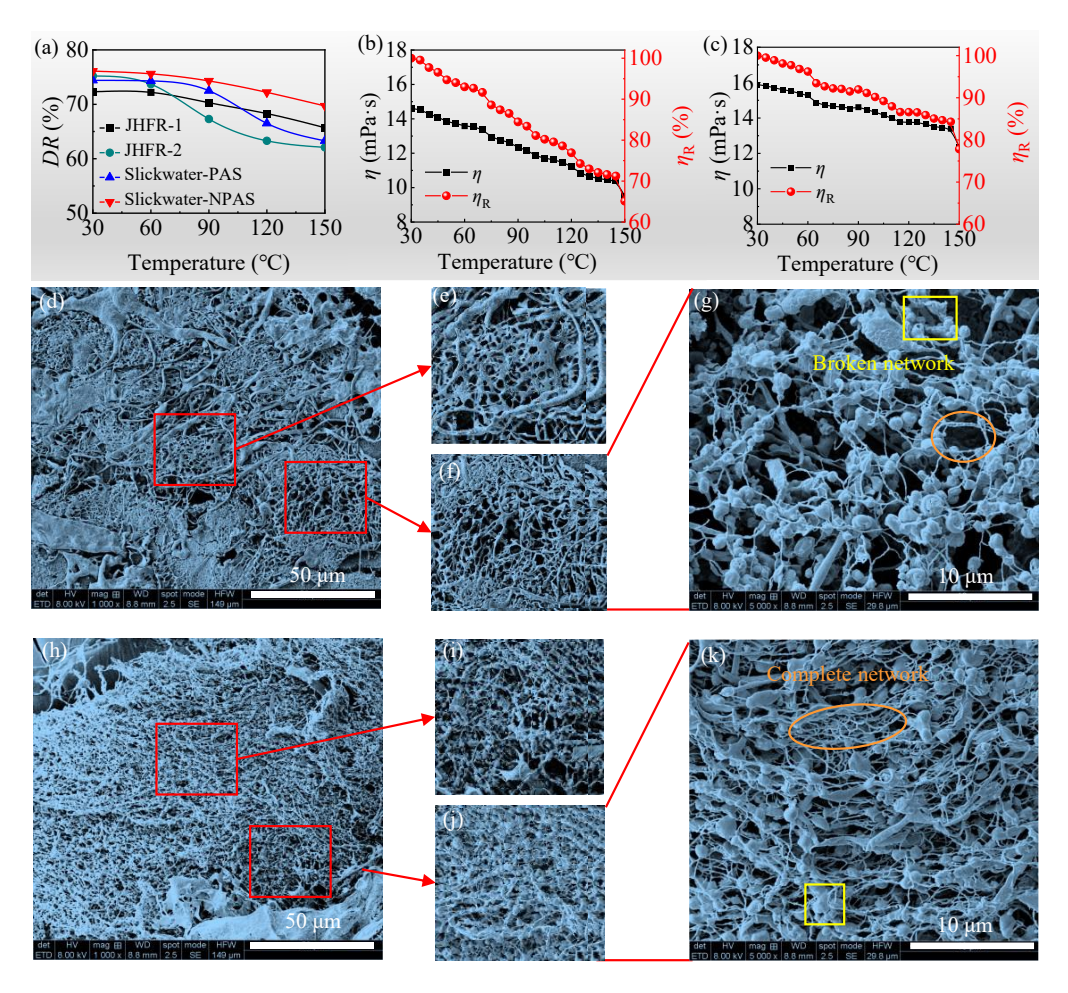


Fig. 9. *DR* curves (a) under different temperatures, viscosity of (b) Slickwater-PAS and (c) Slickwater-NPAS at different temperatures, and morphology of (d)-(g) Slickwater-PAS and (h)-(k) Slickwater-NPAS after aging at 150 °C.

average electrostatic energy calculated over the same 100 ps period was -2.1×10^4 kcal/mol (Fig. 10(h)).

The above findings collectively explain the observed network densification and enhanced thermal resistance, which are attributed to two primary mechanisms (Fig. 10(i)) (Zaragoza et al., 2015; Zareie et al., 2019; Xu et al., 2022): (1) The amide groups of PAS form multiple hydrogen bonds with the amino and hydroxyl groups of nanoparticles; and (2) the dissociated sulfonic acid groups $(-SO_3^-)$ on PAS are electrostatically attracted to the protonated amino groups $(-NH_3^+)$ on the nanoparticle surface. These interactions collectively restrict polymer chain mobility and stabilize the structure against thermal degradation.

4. Conclusions

In this work, a nano-enhanced slickwater fracturing fluid (Slickwater-NPAS) with excellent drag reduction and proppant transport performance was developed for high-temperature reservoirs (e.g., deep shale reservoirs). The incorporation of aminated nano-silica into the AM-AMPS copolymer (PAS) rendered the polymer network reinforced through synergistic hydrogen bonding and electrostatic interactions, effectively mitigating thermal degradation. The key improvements include: (1) A viscosity retention rate of 77.8% after thermal

aging, compared to 65.1% for non-reinforced system; (2) a DR of 69.7% at 150 °C, representing a 10-percentage-point improvement over the non-reinforced system; and (3) enhanced proppant transport capacity, which reduces the proppant settling area by 21.2% and promotes proppant placement in the distal fracture. The elucidated dual reinforcement mechanism, combining nanoparticle-mediated wall smoothing and turbulence suppression with molecular-level network stabilization, effectively restricts polymer segmental mobility, increasing the T_g by 57.5 °C and enhancing thermal stability. Specifically, NPAS exhibits 18.7% more hydrogen bonds and 23.5% lower segmental mobility than PAS, which stabilizes the polymer against thermal degradation. This work provides a robust framework for designing heat-resistant fracturing fluids for deep reservoirs. Future studies should focus on quantifying the structure-activity relationship between fracturing fluid additives and their application performance, thereby offering more effective guidance for the iterative advancement of fracturing fluid technologies.

Acknowledgements

The authors sincerely appreciate the financial support sponsored by the CNPC Innovation Found (No. 2024DQ02-0127) and the China Postdoctoral Science Foundation – Hubei Joint

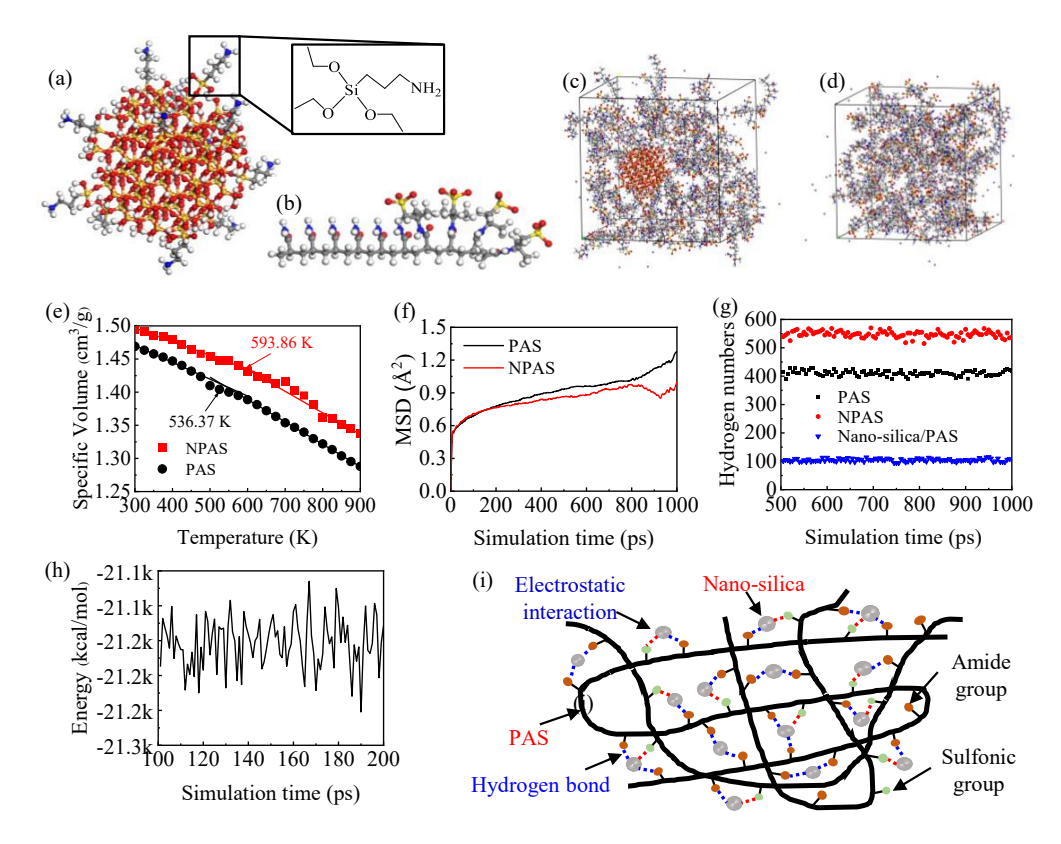


Fig. 10. Molecular configurations of (a) aminated nano-silica and (b) PAS, simulation box models of (c) NPAS and (d) PAS, (e) T_g and (f) MSD curves of NAPS and PAS, (g) hydrogen bonding and (h) electrostatic attraction between nanoparticles and PAS, and (i) schematic of interactions between nanoparticles and PAS.

Support Program (No. 2025T033HB).

Conflict of interest

The authors declare no competing interest.

Open Access This article is distributed under the terms and conditions of the Creative Commons Attribution (CC BY-NC-ND) license, which permits unrestricted use, distribution, and reproduction in any medium, provided the original work is properly cited.

References

Alotaibi, M. A., Miskimins, J. L. Slickwater proppant transport in hydraulic fractures: New experimental findings and scalable correlation. SPE Production & Operations, 2018, 33(2): 164-178.

Asidin, M. A., Suali, E., Jusnukin, T., et al. Review on the applications and developments of drag reducing polymer in turbulent pipe flow. Chinese Journal of Chemical Engineering, 2019, 27(8): 1921-1932.

Brostow, W. Drag reduction in flow: Review of applications, mechanism and prediction. Journal of Industrial and Engineering Chemistry, 2008, 14(4): 409-416.

Cao, J., Song, T., Zhu, Y., et al. Application of aminofunctionalized nanosilica in improving the thermal stability of acrylamide-based polymer for enhanced oil recovery. Energy & Fuels, 2018, 32(1): 246-254.

Ding, F., Dai, C., Sun, Y., et al. A new temperature-resistant and fast dissolving nano-silica/poly (am-amps) composite

drag reducer for slickwater fracturing. Journal of Molecular Liquids, 2023, 387: 122678.

Dunlop, E. H., Cox, L. R. Influence of molecular aggregates on drag reduction. The Physics of Fluids, 1977, 20(10): S203-S213.

Ghannam, M. T., Esmail, M. N. Rheological properties of aqueous polyacrylamide solutions. Journal of Applied Polymer Science, 1998, 69(8): 1587-1597.

Giraldo, L. J., Giraldo, M. A., Llanos, S., et al. The effects of SiO₂ nanoparticles on the thermal stability and rheological behavior of hydrolyzed polyacrylamide based polymeric solutions. Journal of Petroleum Science and Engineering, 2017, 159: 841-852.

Haruna, M. A., Gardy, J., Yao, G., et al. Nanoparticle modified polyacrylamide for enhanced oil recovery at harsh conditions. Fuel, 2020, 268: 117186.

Hu, X., Zhao, X., Ke, Y. Effects of silica nanoparticle on the solution properties of hydrophobically associating polymer based on acrylamide and β -cyclodextrin. Journal of Molecular Liquids, 2019, 296: 111885.

Ibrahim, A. F., Nasr-El-Din, H. A., Rabie, A., et al. A new friction-reducing agent for slickwater-fracturing treatments. SPE Production & Operations, 2018, 33(3): 583-595

Isah, A., Hiba, M., Al-Azani, K., et al. A comprehensive review of proppant transport in fractured reservoirs: Experimental, numerical, and field aspects. Journal of Natural Gas Science and Engineering, 2021, 88: 103832.

- Jouenne, S., Anfray, J., Cordelier, P. R., et al. Degradation (or lack thereof) and drag reduction of HPAM solutions during transport in turbulent flow in pipelines. Oil and Gas Facilities, 2015, 4(1): 80-92.
- Kamel, A., Shah, S. N. Effects of salinity and temperature on drag reduction characteristics of polymers in straight circular pipes. Journal of Petroleum Science and Engineering, 2009, 67(1-2): 23-33.
- Kulicke, W. M., Kniewske, R., Klein, J. Preparation, characterization, solution properties and rheological behaviour of polyacrylamide. Progress in Polymer Science, 1982, 8(4): 373-468.
- Lei, Q., Weng, D., Guan, B., et al. Shale oil and gas exploitation in china: Technical comparison with US and development suggestions. Petroleum Exploration and Development, 2023, 50(4): 944-954.
- Lewandowska, K. Comparative studies of rheological properties of polyacrylamide and partially hydrolyzed polyacrylamide solutions. Journal of Applied Polymer Science, 2007, 103(4): 2235-2241.
- Li, J., Tao, X., Bai, B., et al. Geological conditions, reservoir evolution and favorable exploration directions of marine ultra-deep oil and gas in China. Petroleum Exploration and Development, 2021, 48(1): 60-79.
- Liu, F., Yao, H., Liu, Q., et al. Nano-silica/polymer composite as filtrate reducer in water-based drilling fluids. Colloids and Surfaces A: Physicochemical and Engineering Aspects, 2021, 627: 127168.
- Liu, J., Wang, S., Wang, C., et al. Influence of nanomaterial morphology of guar-gum fracturing fluid, physical and mechanical properties. Carbohydrate Polymers, 2020, 234: 115915.
- Ou, Z., Zhou, Z., Zhou, W., et al. Hierarchical nested riblet surface for higher drag reduction in turbulent boundary layer. Physics of Fluids, 2024, 36(10): 105166.
- Shetty, A. M., Solomon, M. J. Aggregation in dilute solutions of high molar mass poly(ethylene) oxide and its effect on polymer turbulent drag reduction. Polymer, 2009, 50(1): 261-270.
- Tao, J., Meng, S., Li, D., et al. Analysis of CO₂ effects on porosity and permeability of shale reservoirs under different water content conditions. Geoenergy Science and Engineering, 2023, 226: 211774.
- Wang, F., Xu, H., Wang, S., et al. Fluid flow and efficient development technologies in unconventional reservoirs: State-of-the-art methods and future perspectives. Advances in Geo-Energy Research, 2024, 12(3): 237-240.
- Xi, L. Turbulent drag reduction by polymer additives: Fundamentals and recent advances. Physics of Fluids, 2019, 31(12): 121302.
- Xiong, B., Loss, R. D., Shields, D., et al. Polyacrylamide degradation and its implications in environmental systems. npj Clean Water, 2018, 1(1): 17.
- Xu, H., Li, Y., Yu, G., et al. The enhancement of performance and imbibition effect of slickwater-based fracturing fluid by using MoS₂ nanosheets. Petroleum Science, 2023a, 20(4): 2187-2201.

- Xu, P., Shang, Z., Yao, M., et al. Mechanistic insight into improving strength and stability of hydrogels via nanosilica. Journal of Molecular Liquids, 2022, 357: 119094.
- Xu, Z., Zhao, M., Zhang, Y., et al. Bio-inspired superhydrophobic interface of nano-gaseous film for reducing injection pressure in oil reservoirs. Chemical Engineering Journal, 2023b, 454: 140393.
- Yang, B., Zhao, J., Mao, J., et al. Review of friction reducers used in slickwater fracturing fluids for shale gas reservoirs. Journal of Natural Gas Science and Engineering, 2019, 62: 302-313.
- Yang, J., Han, C., Duan, J., et al. Interaction of silica nanoparticle/polymer nanocomposite cluster network structure: Revisiting the reinforcement mechanism. The journal of physical chemistry C, 2013, 117(16): 8223-8230.
- Yegane, M. M., Hashemi, F., Vercauteren, F., et al. Rheological response of a modified polyacrylamide-silica nanoparticles hybrid at high salinity and temperature. Soft Matter, 2020, 16(44): 10198-10210.
- Yuan, S., Zhou, F., Li, Y., et al. A comprehensive study on the enhancements of rheological property and application performances for high viscous drag reducer by adding diluted microemulsion. Geoenergy Science and Engineering, 2023, 227: 211770.
- Zaragoza, J., Babhadiashar, N., O'Brien, V., et al. Experimental investigation of mechanical and thermal properties of silica nanoparticle-reinforced poly(acrylamide) nanocomposite hydrogels. PLoS One, 2015, 10(8): e0136293.
- Zareie, C., Bahramian, A. R., Sefti, M. V., et al. Network-gel strength relationship and performance improvement of polyacrylamide hydrogel using nano-silica; with regards to application in oil wells conditions. Journal of Molecular Liquids, 2019, 278: 512-520.
- Zhang, L., Dai, S., Dai, H., et al. Fast-dissolving twin-tail hydrophobic association polymers drag reducer with salt endurable and shear resistant for slick-water fracturing fluids. Colloids and Surfaces A: Physicochemical and Engineering Aspects, 2025a, 709: 136171.
- Zhang, T., Yang, J., Li, Z., et al. Nano-SiO₂ enhanced slick-water fracturing fluid for improved imbibition recovery in tight gas reservoirs: Performance and mechanism. Colloids and Surfaces A: Physicochemical and Engineering Aspects, 2025b, 707: 135840.
- Zhang, X., Duan, X., Muzychka, Y. Degradation of flow drag reduction with polymer additives a new molecular view. Journal of Molecular Liquids, 2019, 292: 111360.
- Zhao, M., Ma, Z., Dai, C., et al. Preparation and performance evaluation of the slickwater using novel polymeric drag reducing agent with high temperature and shear resistance ability. Petroleum Science, 2024, 21(2): 1113-1121.
- Zuo, C., Liu, P., Du, J., et al. A review: Supramolecular polymers used in high-temperature fracturing fluids research status and prospects on the coupling relationship between molecular conformation and temperature resistance mechanism. Geoenergy Science and Engineering, 2025, 247: 213699.